Microchimica Acta (2019) 186:559
https://doi.org/10.1007/s00604-019-3612-5

ORIGINAL PAPER

A triply amplified electrochemical lead(II) sensor by using a DNAzyme and via formation of a DNA-gold nanoparticle network induced by a catalytic hairpin assembly

Xiaolei Song[1] · Yu Wang[2] · Su Liu[1] · Xue Zhang[2] · Jingfeng Wang[2] · Haiwang Wang[2] · Fenfen Zhang[1] · Jinghua Yu[3] · Jiadong Huang[2,3]

Received: 26 February 2019 / Accepted: 14 June 2019

Abstract

An amplified electrochemical biosensing scheme is described for lead(II) ions. It is making use of DNAzyme-assisted target recycling and catalytic hairpin assembly (CHA). The hairpin strand (substrate probe for the Pb^{2+}-based DNAzyme; referred to as SP) is composed of trigger probe (TP) and a capture probe 1 attached to gold nanoparticles (AuNP). In the presence of the enzyme probe that partially hybridizes with SP, the introduction of Pb^{2+} triggers target recycling and drives the highly amplified translation of target Pb(II) to TP. The CHA reaction is further initiated by TP. The modified AuNP act as the connecting unit, and this leads to the formation of a 3D DNA-AuNP network on the electrode (which is the third amplification step). It can bind the positively charged redox mediator RuHex via electrostatic interaction for electrochemical detection. This biosensor has a low detection limit (95 pM) and any analytical range that covers the 100 pM to 5 μM Pb(II) concentration range. It is selective over other divalent metal ions. It was applied to the determination of Pb^{2+} in spiked real-world samples.

Keywords Lead ion · Electrochemical · Biosensor · DNAzyme · Hairpin-shaped substrate probe · Triple signal amplification · Catalytic hairpin assembly · 3D DNA-AuNP network · RuHex · Real water samples

Introduction

As a well-known and non-biodegradable environmental pollutant, lead cation (Pb^{2+}) can accumulate in human body through the food chain and cause many adverse effects on the immune, central nervous, and reproductive systems, particularly on children [1]. Nowadays, legal restrictions limit the lead level in the environment. According to the International Agency for Research on Cancer (IARC) and the U.S. Environmental Protection Agency (EPA), the thresholds of Pb^{2+} in drinking water are 10 ppb (48.26 nM) and 15 ppb (72 nM), respectively [2]. Therefore, as a public health concern, the development of routine and effective sensing platform for sensitive and selective determination of Pb^{2+} is very essential for water quality control and industrial monitoring. To achieve this, numerous common detection technologies such as atomic absorption spectrometry (AAS) [3], inductively coupled plasma-mass spectrometry (ICP-MS) [4], inductively coupled plasma-atomic emission spectrometry (ICP-AES) [5] have widely been applied in Pb^{2+} determination. However, those methods are still limited by tedious time-consuming sample pretreatment and skilled personnel for on-site detection. During the past decade, although great efforts have been made to improve Pb^{2+} detection performance, there are still challenges that need to be overcome to develop an efficient and convenient method for Pb^{2+} monitoring.

DNAzymes are specific DNA sequences that can recognize target analytes or catalyze specific chemical and biological

Electronic supplementary material The online version of this article (https://doi.org/10.1007/s00604-019-3612-5) contains supplementary material, which is available to authorized users.

✉ Su Liu
stu_lius@ujn.edu.cn

[1] School of Water Conservancy and Environment, University of Jinan, Jinan 250022, People's Republic of China

[2] College of Biological Sciences and Technology, University of Jinan, Jinan 250022, People's Republic of China

[3] Key Laboratory of Chemical Sensing & Analysis in Universities of Shandong, College of Chemistry and Chemical Engineering, University of Jinan, Jinan 250022, People's Republic of China

Published online: 23 July 2019

reactions [6], such as DNA/RNA ligation [7], cleavage [8]. DNAzymes offer advantages over ribozymes or proteins as they have higher catalytic activity and are much more stable [9], that have been successfully employed for the metal ions detection [10, 11]. As a classical model, the typical Pb^{2+}-dependent DNAzyme called "8–17" comprises of a substrate strand (17DS) and an enzyme strand (17E), and the substrate strand containing a single RNA base (rA) at the cleavage site can be cleaved into two pieces in the presence of Pb^{2+} which acts as a cofactor (Scheme 1a) [12]. And the activity of DNAzyme is positively correlated to the concentration of Pb^{2+} [13]. Based on that, some considerable DNAzyme-mediated Pb^{2+} electrochemical biosensors combined with the effective signal amplification means, which overcome the limitations of the traditional protocols, have received increasing attention. For instance, Zhuang et al. developed an electrochemical biosensor by coupling Pb^{2+}-dependent DNAzyme cleavage with hybridization chain reaction (HCR), in which ferrocene (Fc, electrochemical signal tag) was labeled on the formed DNA nanowires [14]. Liu and co-workers reported an electrochemical DNAzyme biosensor for Pb^{2+} using cleavage-induced template-independent polymerization (using terminal deoxynucleotidyl transferase, TdTase) and alkaline phosphatase amplification [15]. Cai et al. studied a miniaturized electrochemical biosensing system for Pb^{2+} detection based on dual Pb^{2+}-DNAzyme assistant feedback strategy, which involves two rolling circle amplification (RCA) processes [16]. Nevertheless, compared with other strategies, the Fc labeling procedure and enzymes all make the detection relatively costly and complicated. Therefore, it is highly desirable to get access to a highly sensitive approach for Pb^{2+} assay that offers the advantages of excellent stability performance in real-life sample analysis.

Poly adenine (poly A) sequences containing multiple consecutive adenines, as an elaborate anchoring block for preferential binding with the gold nanoparticles (AuNP) surface with high affinity, even comparable to gold-thiol chemistry. And poly A-mediated binding requires no modification during synthesis, inducing easy modulation in the preparation of DNA-AuNP conjugates with high purity and low cost [17, 18]. More interestingly, catalytic hairpin assembly (CHA), as a simple nucleic-acid amplifying strategy, can effectively amplify signal from branched DNA junctions fabricated by the trigger-initiated circular assembly of metastable hairpin probes without the involvement of enzyme. It can offer unique features for point-of-case analyte detection with negligible background [19, 20].

As a proof-of-concept experiment, herein, a novel electrochemical method for Pb^{2+} analysis with the combination of DNAzyme as a recognition element, and AuNP and CHA as the signal amplification tools has been first reported. The construction process and biosensing principle of this strategy is outlined in Scheme 1, including three steps: (A) the DNAzyme-based Pb^{2+} recycling amplification; (B) the CHA reaction; (C) self-assembly of 3D DNA-AuNP network on gold electrode (AuE) and the electrochemical assay. In the first step, the constructed SP-AuNP involves a properly designed hairpin-shaped probe (substrate probe of the DNAzyme, SP),

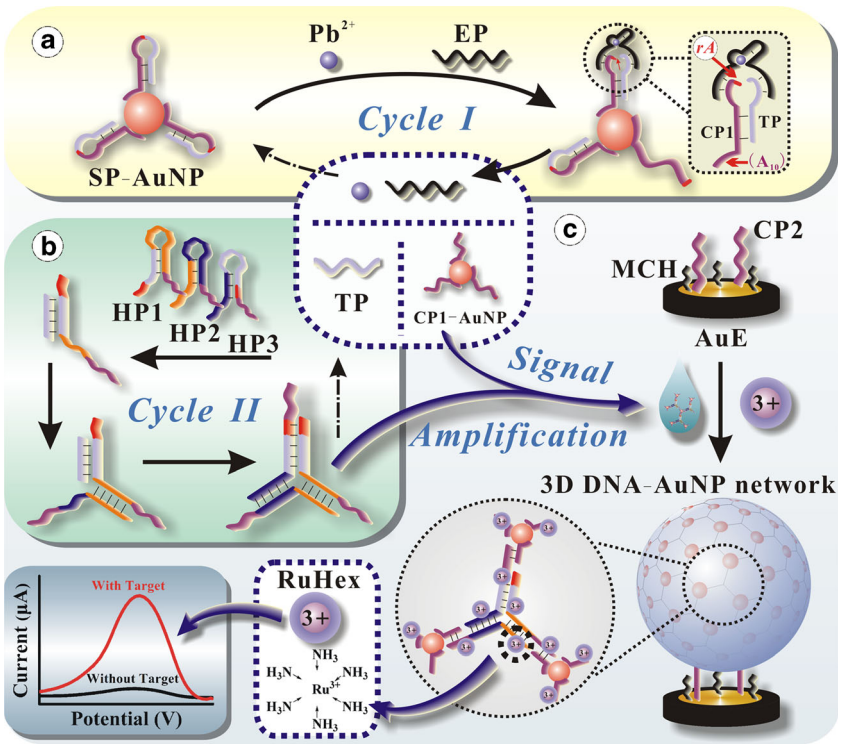

Scheme 1 Schematic illustration of the electrochemical biosensor for Pb^{2+} determination

which conjugate to the AuNP via poly A_{10}. The enzyme probe (EP) can partially hybridizes with SP-AuNP to form the DNAzyme system. Upon the participation of the cofactor Pb^{2+}, the DNAzyme is cleaved at the rA position, bringing about the release of target Pb^{2+}, EP, and two fragments of SP-AuNP that serves as trigger probe (TP) and capture probe 1 (CP1-AuNP), respectively. The liberated Pb^{2+} and EP can then hybridize with another SP-AuNP to achieve the first cycle cleavage (Cycle I). In the second one, the released TP triggers CHA reaction between three alternating hairpin DNA probes (HP1, HP2 and HP3), that contain the complementary strands (purple parts) of CP1, to form the branched DNA junctions (*Note*: The procedure of CHA between three hairpins is introduced in detail in Supporting Information), which constitutes Cycle II. In the last, third, the capture probe 2 (CP2) supplied as the substrate for the 3D DNA-AuNP network is immobilized on the AuE surface through Au-S bond [21]. MCH is further assembled on the AuE to block blank binding sites. Subsequently, the CP1-AuNP from Cycle I can hybridize with CP2, then the obtained branched DNA junctions from Cycle II can be assembled on the AuE with the CP1-AuNP through a hybridization reaction. Due to the excellent surface area of AuNP [22], the 3D DNA-AuNP network can be formed after repetitive hybridizations between the branched DNA junctions and CP1-AuNP to afford large amounts of DNA concatemers on the AuE surface. These negative charge DNA concatemers can gather positive charge redox indicators (the third signal amplification), $[Ru(NH_3)_6]^{3+}$ (RuHex for short), via electrostatic interaction, leading to an obvious readout signal [23, 24]. Thus, by using the triple signal amplification process, this inspired biosensor can offer a controllable and economically method for Pb^{2+} determination.

Materials and methods

Materials

Oligonucleotides were HPLC-purified and synthesized by Sangon Biotechnology Co., Ltd. (Shanghai, China; https://www.sangon.com/), and their sequences were listed in Tab. S1. And all hairpin probes were heated to 95 °C for 5 min and then cooled immediately for 15 min in ice bath before use. Lead nitrate ($Pb(NO_3)_2{\cdot}3H_2O$), 6-mercapto-l-hexanol (MCH), trisodium citrate and chloroauric acid ($HAuCl_4{\cdot}4H_2O$) were obtained from Aladdin Chemistry Co., Ltd. (Shanghai, China; http://www.aladdin-e.com/). Hexaammineruthenium (III) chloride ($[Ru(NH_3)_6]^{3+}$, RuHex) was from Sigma-Aldrich Chemical Co. (St. Louis, MO; https://www.sigmaaldrich.com/). All other reagents were of analytical grade and purchased from Sinopharm Chemical Reagent Co., Ltd. (Beijing, China; https://www.sinoreagent.com/). All solutions were prepared using ultrapure water with an electric resistance >18 MΩ·cm that was obtained through a Millipore Milli-Q water purification system (Billerica, MA, USA; http://www.merckmillipore.com/).

Apparatus and characterization

All electrochemical measurements were performed with a CHI 660D electrochemical workstation which purchased from Chen Hua Instrument Co., Ltd. (Shanghai, China; http://www.chinstr.com/) via a conventional three-electrode system. And the three-electrode system composes of a bare or functionalized gold electrode (AuE, 2 mm in diameter) as the working electrode, a platinum wire as the auxiliary electrode, and a Ag/AgCl reference electrode with a saturated KCl solution. Differential pulse voltammetry (DPV) was carried out in 10 mM phosphate buffered saline (PBS, 1×, containing 140 mM NaCl, 5 mM KCl, 1 mM $MgCl_2$, pH 7.4) within the potential range from −0.6 to 0 V with a step potential of 0.83 mV. The modulation amplitude was 50 mV, and the pulse width was 50 mV s^{-1}. Cyclic voltammetry (CV) measurement was performed in 5 mM $[Fe(CN)_6]^{3-/4-}$ aqueous solution containing 0.25 mM KCl in the voltage range from −0.2 to 0.6 V with scan rate of 50 mV s^{-1}. Electrochemical impedance spectroscopy (EIS) measurement was recorded within 5 mM $[Fe(CN)_6]^{3-/4-}$ solution containing 0.25 mM KCl in the frequency range from 0.1 Hz to 100 kHz with an amplitude of 5 mV.

Absorption spectra were conducted on a UV2600 UV-vis spectrophotometer (Shimadzu international trading Co. Ltd., Japan; http://www.shimadzu.com.cn/) in the wavelength range from 400 nm to 800 nm at room temperature. Transmission electron microscopy (TEM) measurement was carried out using a transmission electron microscope (JEM-3010; http://www.jeol.co.jp/). The sample for TEM characterization was prepared by adding a drop of colloidal solution on a carbon-coated copper grid and then drying at room temperature.

Preparation of SP-AuNP

The synthesis process of AuNP (20 nm) was given in the Supporting Information. For preparing SP-AuNP [17], the citrate-stabilized AuNP was incubated with SP (poly A_{10} anchoring block) in a molar ratio (SP/AuNP) of 5000 for 16 h. The mixture was then brought to 10 mM sodium phosphate buffer (pH 7.4) containing 100 mM NaCl, allowed to stand for 40 h. Afterward, the particles were washed three times in 10 mM sodium phosphate buffer (pH 7.4) with 100 mM NaCl through centrifugation (15,000 rpm (21,380 rcf), 10 min, 4 °C) to remove excess SP. Finally, the resulting conjugates were re-dispersed in ultrapure water and stored at 4 °C until use.

Pretreatment and fabrication of the biosensor

Firstly, the working gold electrodes (AuE) were cleaned by immersing in freshly-prepared piranha solution (H_2O_2/H_2SO_4, 1:3) for 2 h with three times, and rinsed with ultrapure water. Then, the AuE were polished on the microcloth with 0.05 μm alumina suspension, followed by ultrasonic cleaning in ethanol and ultrapure water, respectively. Finally, the electrodes were again rinsed thoroughly with ultrapure water and dried under nitrogen stream. Subsequently, 10 μL of thiolated CP2 (0.1 μM) was dropped on the cleaned AuE surface and incubated for 2 h at 37 °C to form self-assembly monolayers by Au-S bond. After rinsing gently with PBS (10 mM, pH 7.4), the AuE was subjected to incubate with 10 μL MCH (2 mM) solution for 2 h to ensure a monolayer of CP2 in a consistent orientation. After that, the resulting MCH/CP2/AuE was thoroughly rinsed with PBS (10 mM, pH 7.4) and stored at 4 °C for ready.

In the meantime, an aqueous solution of Pb^{2+} (2 μL, 0–10 μM, or unknown sample) was mixed with SP-AuNP (4 μL, 1 μM (AuNP was 0.2 nM)), EP (2 μL, 0.1 μM), 1× reaction buffer (50 mM Tris-HCl and 500 mM NaCl, pH 8.2). After incubated at 37 °C for 1 h, HP1, HP2 and HP3 (2 μL, 0.4 μM, respectively) were added with a total volume of 20 μL, and then 10 μL of above solution was attached on the MCH/CP2/AuE for 2 h at 37 °C to form the 3D DNA-AuNP network. Finally, the electrode was reacted with 10 μL of RuHex (50 μM) for 10 min at room temperature to ensure RuHex is stably anchored to the DNA concatemers, and rinsed with PBS (10 mM, pH 7.4) three times for DPV detection.

Results and discussion

Characterization of bare AuNP and SP-AuNP

Transmission electron microscopy (TEM) was utilized to characterize the prepared bare AuNP (Fig. 1a). The spherical structure of AuNP shows homogeneous diameter (~ 20 nm) and good dispersion. Additionally, UV-vis spectroscopy experiments of AuNP with different states were further performed, and revealed in Fig. 1b. The citrate-capped AuNP shows a typical absorption peak with the absorption wavelength at 519 nm (blank line). Upon the addition of SP strand, the characteristic absorption peak of AuNP at 519 nm is red-shifted to 524 nm (red line), which demonstrates the successful accomplishment of the SP-AuNP nanoprobes.

Investigation of the feasibility and multiple signal amplification of the Pb^{2+} biosensor

In order to confirm the feasibility of the designed electrochemical biosensing strategy, under different conditions, differential pulse voltammetry (DPV) responses were detected using RuHex as the indicator and the results are depicted in Fig. 2. For the blank sample, it is clear that the current intensity at around −0.22 V is weak (curve b). In contrast, when the constructed biosensor is incubated in the solution containing 5 μM Pb^{2+}, the DPV response increased largely (curve a, positive sample). It is indicated that a substantial number of RuHex close to the AuE surface by binding to the phosphate backbones of DNA for efficient electron transfer. This clearly reveals that the electrochemical method can be employed only with the target Pb^{2+}. Subsequently, we performed the control experiment differing in EP. In the absence of EP, there is a negligible DPV peak (curve c) similar to that of the blank sample in the DPV curves, confining that CP1 and TP will be caged in the "close" hairpin structure of SP without EP. Then, a poor DPV peak is observed in the presence of counter-target Hg^{2+} instead of Pb^{2+}, demonstrating that the significantly increased DPV signal is relied on the specific recognition of target Pb^{2+} (curve d).

Additionally, to verify the triply amplified strategy of this biosensing platform, we also studied the control experiments through the MCH/CP2-modified AuE immersed

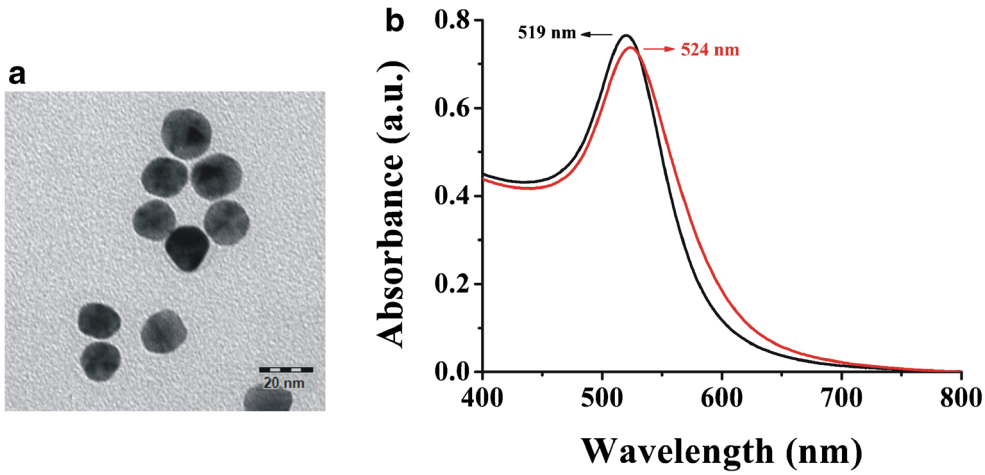

Fig. 1 **a** TEM micrograph of AuNP; **b** absorption spectra of AuNP (blank line) and SP-AuNP (red line)

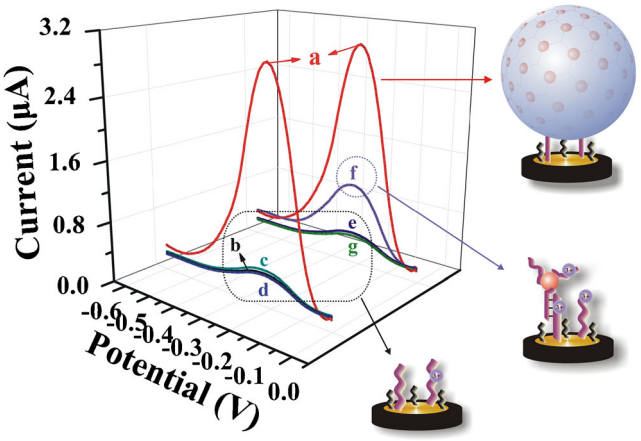

Fig. 2 Typical DPV responses of the electrochemical assay via the exposure of the modified AuE to the positive sample (5 μM Pb^{2+}, (a)), blank sample (b), 5 μM Pb^{2+} without EP (c), 5 mM Hg^{2+} in place of 5 μM Pb^{2+} (d), 5 μM Pb^{2+} without any cycles (e), 5 μM Pb^{2+} with Cycle I only (f), 5 μM Pb^{2+} with Cycle II only (g)

in the solution containing different cycles. There are two poor current intensities without any cycles (curve e) and with Cycle II only (without EP and SP-AuNP, curve g) similar to that of the blank sample (curve b), respectively, showing that there are no obvious amplification effect. When the MCH/CP2-AuE is incubated with Cycle I only (curve f), a moderate DPV peak is observed, suggesting that the assembly of CP1-AuNP on the AuE will lead to slight signal amplification. However, once two cycles were further introduced, the DPV response increased obviously (curve a), which is ascribed to the formation of the 3D DNA-AuNP network, resulting in more negative charges on the AuE. All these results signify that the highest signal is obtained via the dual amplification strategy and the additive amplification efficiency of Cycle I combined with Cycle II is much higher than that of Cycle I only. Therefore, according to the DPV response change, it is reasonably concluded that this amplification route can be feasible for Pb^{2+} assay.

Electrochemical characterization of the modified electrodes

Electrochemical impedance spectroscopy (EIS) reflects the interface feature of the electrode, which can be carried out as a very sensitive tool to validate the stepwise fabrication process of this biosensor. In a typical EIS, the diameter of semicircle corresponds to the electron-transfer resistance (R_{et}), which shows the electron transfer kinetics of the redox probe ($[Fe(CN)_6]^{3-/4-}$) at the AuE surface. As illustrated in Fig. 3a, a very small semicircle is obtained at bare AuE (curve a), indicating a low electron-transfer resistance. The resistance increase with the assembly of CP2 on the electrode (curve b), which is owing to the electrostatic repulsion between negative charges of the DNA oligonucleotides backbone and the negatively charged $[Fe(CN)_6]^{3-/4-}$ ions. Subsequently, after immersing the CP2-modified AuE into the MCH solution (curve c), a higher impedance is achieved, suggesting that MCH is mobilized on the surface of AuE. Especially after the hybridization reaction with 3D DNA-AuNP network in the presence of Pb^{2+}, the resistance dramatically increased (curve d), which shows the access of the redox probe to the electrode is further hindered because of the resistance of DNA. However, when the MCH/CP2/AuE was treated by the solution without Pb^{2+}, the resistance of electrode almost no change (curve e), indicating that the formation of the 3D DNA-AuNP network due to the specific interaction between the biosensor and Pb^{2+}. Furthermore, the changes of the electrode behavior were also characterized by cyclic voltammogram (CV) (shown in Fig. 3b). Compared with the redox peak currents of the bare AuE (curve a), CP2/AuE (curve b) and MCH/CP2/AuE (curve c) slightly decreased, successively. Then, the CV response is obviously inhibited and the peak gap is significantly separated after the surface of electrode is modified with 3D DNA-AuNP network (curve d), which is attributed to the large assembly of the DNA concatemer with negative charges. As expected, the absence of Pb^{2+} leads to a moderate CV signal (curve e) that similar to curve c, revealing that the generation of the

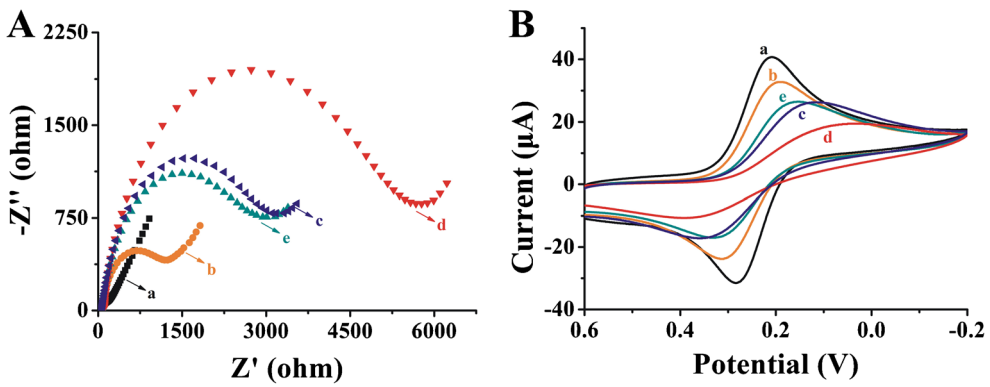

Fig. 3 Nyquist plots (**A**) and CVs (**B**) of the biosensor assembly process. (a) bare AuE, (b) CP2/AuE, (c) MCH/CP2/AuE, (d) 3D DNA-AuNP network/MCH/CP2/AuE, (e) MCH/CP2/AuE incubated with the solution without Pb^{2+}. The concentration of Pb^{2+} is 5 μM

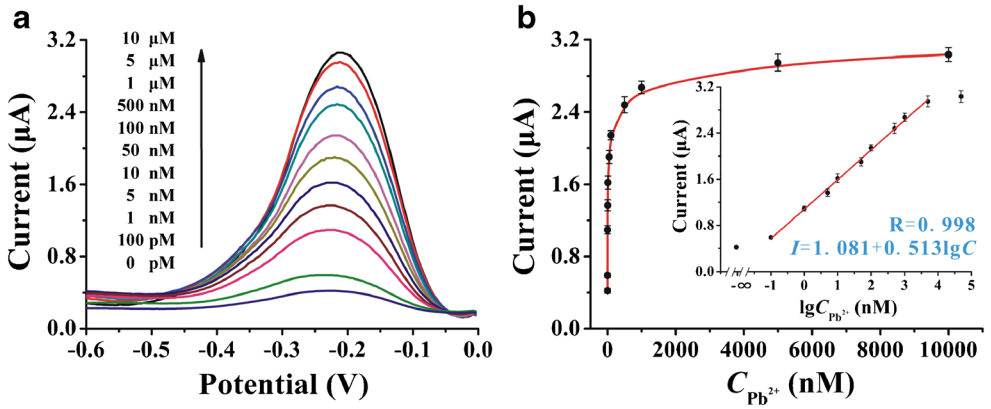

Fig. 4 **a** The DPV responses of the electrochemical biosensor versus Pb^{2+} with various concentrations (0, 0.1×10^0, 1×10^0, 5×10^0, 1×10^1, 5×10^1, 1×10^2, 5×10^2, 1×10^3, 5×10^3, 1×10^4 nM); **b** plots of current signal vs different concentrations of Pb^{2+}. Inset: the relationship between DPV peak and the logarithm of Pb^{2+} concentration in the range from 100 pM to 5 μM. Error bars show the standard deviations across three repetitive experiments

3D DNA-AuNP network after the specific cleavage of Pb^{2+}. Thus, the results are in accordance with that observed in EIS value as confirmation of the successful construction of the electrochemical biosensor.

Analytical performance of the prepared biosensor toward Pb^{2+}

To explore the quantitative application of this electrochemical biosensor, this prepared method was employed for various concentration of Pb^{2+} under the optimal conditions (see Supporting Information). As seen in Fig. 4a, the DPV response of the biosensor enhances gradually corresponding to the concentration of Pb^{2+} increased from 0 to 10 μM. Furthermore, the current intensity continues to increase with the increasing concentration of Pb^{2+} until reaching a plateau, as displayed in Fig. 4b. And the DPV value is proportional to the logarithm (lg) of Pb^{2+} in the concentration range 100 pM-5 μM, with a linear regression equation expressed as $I = 1.081 + 0.513\ \lg C$ (I and C stand for the peak current intensity and the concentration of Pb^{2+}, respectively) and the correlation coefficient is R = 0.998 (Inset in Fig. 4b). The limit of detection (LOD) is calculated to be 95 pM based on evaluating the average response of blank sample plus 3 times standard deviation. Additionally, in comparison with other existing approaches (as listed in Table 1), this reported system for Pb^{2+} exhibits a lower detection limit and the wider range, which is attributed to the triply amplified strategy, suggesting that the promising avenue of the biosensor in potable water.

From the practical point, selectivity is the essential element for Pb^{2+} exploration. Under the optimized analysis conditions, control experiments were examined by challenging the assay against several environmentally relevant divalent metal ions including Cu^{2+}, Mg^{2+}, Ca^{2+}, Hg^{2+}, Zn^{2+}, Mn^{2+}, Cd^{2+} and Ni^{2+} (5 mM, respectively), which are commonly coexist with Pb^{2+}. As revealed in Fig. 5, compared with the blank sample, the interfering metal ions cannot cause any distinct DPV change, while an obviously high current signal is observed in the presence of Pb^{2+} (5 μM) only. In addition, the response of Pb^{2+} coexisted with the non-target metal ions is similar to those without interfering ions. The above consequence demonstrates the excellent specificity of this biosensing platform for Pb^{2+}.

Reproducibility, another important parameter, was also employed to evaluate the performance of the biosensor. The relative standard deviation (RSD) obtained by five constructed biosensors incubated with 5 μM Pb^{2+} was 3.4%, illustrating this biosensor has an acceptable reproducibility. In addition, a long-term storage assay was further studied for the stability of our biosensor, by measuring the DPV signal for 5 μM Pb^{2+} at regular intervals (2 days). After 2 weeks, the

Table 1 Detection performance comparison of our assay with other methods

Strategies [a]	Methods [b]	Linear range (pM)	LOD (pM)	Ref.
D/GLSS	*C*	2.0×10^3–1.0×10^6	2.0×10^3	[25]
G/CD	*C*	1.0×10^3–8.0×10^5	1.0×10^3	[26]
D/AgNC	*F*	5.0×10^3–5.0×10^4	1.0×10^3	[27]
D/SDR	*F*	1.0×10^3–1.0×10^6	3.0×10^2	[28]
D/Z	*PE*	5.0×10^2–2.0×10^4	1.0×10^2	[29]
D/AuNP	*SERS*	1.0×10^3–1.0×10^7	1.0×10^3	[30]
D	*E*	5.0×10^2–5.0×10^6	2.5×10^2	[31]
D/CHA/AuNP	*E*	1.0×10^2–5.0×10^6	9.5×10^1	This work

[a] *D* DNAzyme, *GLSS* gold label silver stain, *G* G-quadruplexes, *CD* cliplike cyanine dye, *AgNC* silver nanoclusters, *SDR* strand displacement reaction, *Z* ZnO nanoflower

[b] *C* colorimetric, *F* fluorescence, *PE* photoelectrochemical, *SERS* surface enhanced Raman scattering, *E* electrochemical

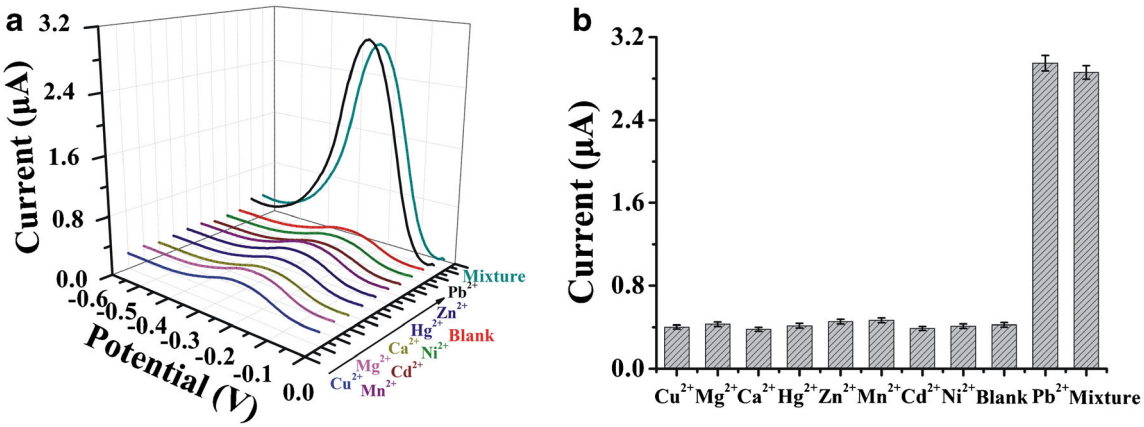

Fig. 5 **a** DPV responses and **b** histogram of the electrochemical biosensor toward target Pb^{2+} (5 μM) against Cu^{2+}, Mg^{2+}, Ca^{2+}, Hg^{2+}, Zn^{2+}, Mn^{2+}, Cd^{2+} and Ni^{2+} (5 mM, respectively). Error bars are standard deviations across three repetitive experiments

biosensor retained 93% of its initial current response, indicating a good stability of the designed biosensor.

Practical application

The applicability of the fabricated electrochemical strategy in water sample (tap water was used without further treatment), which obtained from our laboratory, was successfully implemented. The existing Pb^{2+} in tap water cannot be detected by our biosensor. Then, Pb^{2+} ions were added into the tap water samples at three different concentrations of 5 nM, 50 nM and 100 nM according to the standard addition method. These samples were measured using our biosensor and the classic inductively coupled plasma-mass spectrometry (ICP-MS), respectively. It is observed from Tab. S2 that these data obtained by our strategy reveal a good agreement with those determined via ICP-MS. And the discrepancies between the two methods are all less than 12.4%. This clearly demonstrates that the established biosensor may be applied for real water sample analysis with excellent accuracy and reliability.

Conclusions

In summary, a bio-inspired DNAzyme-based triple-signal amplification strategy was established to construct electrochemical biosensor for the detection of Pb^{2+}. The ingenious Pb^{2+}-based DNAzyme as the recognition element exhibits excellent specificity, while our assay brights about high sensitivity due to following reasons: First, a doubly amplified strategy using DNAzyme and catalytic hairpin assembly is capable of generating amounts of branched DNA junctions; Second, AuNP with large surface area directly served as an efficient linker for the formation of 3D DNA-AuNP network (the third amplification) to bind with RuHex, which triggers significant enhancement of electrochemical signal. With outstanding design, this method provides a potential platform for Pb^{2+} detection in real water sample, and our future works will be aimed at creating the simpler electrochemical biosensors without redox mediators.

Acknowledgements This work was supported by National Natural Science Foundation of China (31471644), the Primary Research & Development Plan of Shandong Province (2017GSF220009), the Program for Taishan Scholer of Shandong Province (TS201712048), University of Jinan Scientific Research Fund (Youth Project XKY1421) and Doctoral Fundation of University of Jinan (XBS1431).

Compliance with ethical standards The author(s) declare that they have no competing interests.

References

1. Dong JP, Fang QH, He HB, Zhang Y, Xu JQ, Sun YB (2015) Electrochemical sensor based on EDTA intercalated into layered double hydroxides of magnesium and aluminum for ultra trace level detection of lead (II). Microchim Acta 182(3–4):653–659
2. Wang LL, Wen YL, Li LY, Yang X, Jia NQ, Li W, Meng JR, Duan ML, Sun XG, Liu G (2018) Sensitive and label-free electrochemical lead ion biosensor based on a DNAzyme triggered G-quadruplex/hemin conformation. Biosens Bioelectron 115:91–96
3. Ghaedi M, Ahmadi F, Shokrollahi A (2007) Simultaneous preconcentration and determination of copper, nickel, cobalt and lead ions content by flame atomic absorption spectrometry. J Hazard Mater 142(1–2):272–278
4. Shum SCK, Pang HM, Houk RS (1992) Speciation of mercury and lead compounds by microbore column liquid chromatography-inductively coupled plasma mass spectrometry with direct injection nebulization. Anal Chem 64(20):2444–2450
5. Badiei HR, Liu C, Karanassios V (2013) Taking part of the lab to the sample: on-site electrodeposition of Pb followed by measurement in a lab using electrothermal, near-torch vaporization sample introduction and inductively coupled plasma-atomic emission spectrometry. Microchem J 108:131–136
6. Wang HL, Ou LML, Suo YR, Yu HZ (2011) Computer-readable DNAzyme assay on disc for ppb-level lead detection. Anal Chem 83(5):1557–1563
7. Wang YM, Silverman SK (2005) Efficient one-step synthesis of biologically related lariat RNAs by a deoxyribozyme. Angew Chem Int Ed 44(36):5863–5866

8. Faulhammer DCD, Famulok PDM (1996) The Ca^{2+} ion as a cofactor for a novel RNA-cleaving deoxyribozyme. Angew Chem Int Ed Eng 35(23–24):2837–2841
9. Yun W, Cai DZ, Jiang JL, Zhao PX, Huang Y, Sang G (2016) Enzyme-free and label-free ultra-sensitive colorimetric detection of Pb^{2+} using molecular beacon and DNAzyme based amplification strategy. Biosens Bioelectron 80:187–193
10. Liu JW, Lu Y (2004) Accelerated color change of gold nanoparticles assembled by DNAzymes for simple and fast colorimetric Pb^{2+} detection. J Am Chem Soc 126(39):12298–12305
11. Yun W, Du XQ, Liao JS, Sang G, Chen L, Li N, Yang LZ (2018) Three-way DNA junction based platform for ultra-sensitive fluorometric detection of multiple metal ions as exemplified for Cu(II), Mg(II) and Pb(II). Microchim Acta 185:306. https://doi.org/10.1007/s00604-018-2836-0
12. Mazumdar D, Nagraj N, Kim HK, Meng XL, Brown AK, Sun Q, Li W, Lu Y (2009) Activity, folding and Z-DNA formation of the 8-17 DNAzyme in the presence of monovalent ions. J Am Chem Soc 131(15):5506–5515
13. Zhang Y, Wang LJ, Zhang CY (2014) Highly sensitive detection of telomerase using a telomere-triggered isothermal exponential amplification-based DNAzyme biosensor. Chem Commun 50(15):1909–1911
14. Zhuang JY, Fu LB, Xu MD, Zhou Q, Chen GN, Tang DP (2013) DNAzyme-based magneto-controlled electronic switch for picomolar detection of lead (II) coupling with DNA-based hybridization chain reaction. Biosens Bioelectron 45:52–57
15. Liu SF, Wei WJ, Sun XY, Wang L (2016) Ultrasensitive electrochemical DNAzyme sensor for lead ion based on cleavage-induced template-independent polymerization and alkaline phosphatase amplification. Biosens Bioelectron 83:33–38
16. Cai W, Xie SB, Zhang J, Tang DY, Tang Y (2018) Immobilized-free miniaturized electrochemical sensing system for Pb^{2+} detection based on dual Pb^{2+}-DNAzyme assistant feedback amplification strategy. Biosens Bioelectron 117:312–318
17. Pei H, Li F, Wan Y, Wei M, Liu HJ, Su Y, Chen N, Huang Q, Fan CH (2012) Designed diblock oligonucleotide for the synthesis of spatially isolated and highly hybridizable functionalization of DNA-gold nanoparticle nanoconjugates. J Am Chem Soc 134(29):11876–11879
18. Wen JL, Chen JH, Zhuang L, Zhou SG (2016) Designed diblock hairpin probes for the nonenzymatic and label-free detection of nucleic acid. Biosens Bioelectron 79:656–660
19. Li X, Xie JQ, Jiang BY, Yuan R, Xiang Y (2017) Metallo-toehold-activated catalytic hairpin assembly formation of three-way DNAzyme junctions for amplified fluorescent detection of Hg^{2+}. ACS Appl Mater Interfaces 9(7):5733–5738
20. Yu S, Wang YY, Jiang LP, Bi S, Zhu JJ (2018) Cascade amplification-mediated in situ hot-spot assembly for microRNA detection and molecular logic gate operations. Anal Chem 90(7):4544–4551
21. Han C, Li RG, Li H, Liu S, Xu CG, Wang JF, Wang Y, Huang JD (2017) Ultrasensitive voltammetric determination of kanamycin using a target-triggered cascade enzymatic recycling couple along with DNAzyme amplification. Microchim Acta 184(8):2941–2948
22. Yang XR, Xu J, Tang XM, Liu HX, Tian DB (2010) A novel electrochemical DNAzyme sensor for the amplified detection of Pb^{2+} ions. Chem Commun 46(18):3107–3109
23. Shen L, Chen Z, Li YH, He SL, Xie SB, Xu XD, Liang ZW, Meng X, Li Q, Zhu ZW, Li MX, Le XC, Shao YH (2008) Electrochemical DNAzyme sensor for lead based on amplification of DNA-Au bio-bar codes. Anal Chem 80(16):6323–6328
24. Wang ZH, Sun N, He Y, Liu Y, Li JH (2014) DNA assembled gold nanoparticles polymeric network blocks modular highly sensitive electrochemical biosensors for protein kinase activity analysis and inhibition. Anal Chem 86(12):6153–6159
25. Chen BB, Wang ZB, Hu DX, Ma QQ, Huang LN, Xv CY, Guo ZY, Jiang XH (2014) Scanometric nanomolar lead (II) detection using DNA-functionalized gold nanoparticles and silver stain enhancement. Sensor Actuat B-Chem 200:310–316
26. Sun HX, Yu LJ, Chen HB, Xiang JF, Zhang XF, Shi YH, Yang QF, Guan AJ, Li Q, Tang YL (2015) A colorimetric lead (II) ions sensor based on selective recognition of G-quadruplexes by a clip-like cyanine dye. Talanta 136:210–214
27. Gong L, Kuai HL, Ren SL, Zhao XH, Huan SY, Zhang XB, Tan WH (2015) Ag nanocluster-based label-free catalytic and molecular beacons for amplified biosensing. Chem Commun 51(60):12095–12098
28. Wen ZB, Liang WB, Zhuo Y, Xiong CY, Zheng YN, Yuan R, Chai YQ (2017) An efficient target-intermediate recycling amplification strategy for ultrasensitive fluorescence assay of intracellular lead ions. Chem Commun 53(54):7525–7528
29. Zhang BT, Lu LL, Hu QC, Huang F, Lin Z (2014) ZnO nanoflower-based photoelectrochemical DNAzyme sensor for the detection of Pb^{2+}. Biosens Bioelectron 56:243–249
30. Fu CC, Xu WQ, Wang HL, Ding H, Liang LJ, Cong M, Xu SP (2014) DNAzyme-based plasmonic nanomachine for ultrasensitive selective surface-enhanced Raman scattering detection of lead ions via a particle-on-a-film hot spot construction. Anal Chem 86(23):11494–11497
31. Zhang YL, Xiao SX, Li HZ, Liu HJ, Pang PF, Wang HB, Wu Z, Yang WR (2016) A Pb^{2+}-ion electrochemical biosensor based on single-stranded DNAzyme catalytic beacon. Sensor Actuat B-Chem 222:1083–1089